

Contents lists available at ScienceDirect

# Combustion and Flame

journal homepage: www.elsevier.com/locate/combustflame



# Impacts of preferential vaporization on flashback behaviors of multi-component liquid fuels



Seung Jae Lim, Ayuob K. Alwahaibi, Frederick L. Dryer, Sang Hee Won\*

Department of Mechanical Engineering, University of South Carolina, Columbia, SC 29208, USA

#### ARTICLE INFO

Article history:
Received 10 February 2022
Revised 11 July 2022
Accepted 12 July 2022
Available online 1 August 2022

Keywords: Preferential vaporization Flame flashback Low-temperature ignition

#### ABSTRACT

Liquid transportation fuels are composed of a wide range of molecular structures and weights, therefore exhibiting a relatively large distillation temperature range. When fuel chemical properties change along with the distillation temperature curve, preferential vaporization effects could play a role in near-limit combustion behaviors. The objective of this study is to experimentally evaluate the role of preferential vaporization on flame flashback behaviors. A unique spray burner is developed to control the extent of fuel spray vaporization by adjusting flow rates and/or the spray injection location from the burner exit. Spray characteristics are comprehensively determined using Phase Doppler Particle Analyzer. Two binary component mixtures are formulated (n-octane/iso-cetane and iso-octane/n-hexadecane) to exhibit common combustion behaviors in the fully vaporized condition but have considerably different preferential vaporization characteristics. Identical flashback behaviors of two mixtures are observed for fully pre-vaporized conditions by setting the burner temperature at 700 K, including both propagation- and ignition-driven flashback behaviors. Partially vaporized conditions are investigated at two global equivalence ratios (1.0 and 1.4) by setting the burner temperature at 450 K. The flashback behaviors for both global equivalence ratio conditions are found to be affected by the preferential vaporization characteristics represented by laminar flame speeds of the vaporized fuel mixture composition. The relative significance of local flow perturbation induced by instantaneous fuel droplet evaporation near the flame surface has been also investigated by analyzing planar laser-induced fluorescence images, as well as considering the changes of Markstein length with the extent of fuel vaporization. Finally, the relative contributions of local laminar flame speed representing local fuel vapor deposit, local flow perturbation, and preferential vaporization are evaluated through feature sensitivity analyses.

 $\ensuremath{\mathbb{C}}$  2022 The Combustion Institute. Published by Elsevier Inc. All rights reserved.

# 1. Introduction

The multi-phase combustion behaviors of real liquid fuels in energy conversion devices, particularly at near-limit conditions, are dependent on fuel physical and chemical properties [1] by their coupling effects on chemical kinetic characteristics, spray dynamics, turbulent mixing, and heat transfer phenomena [2–9]. Regarding gas turbine combustion, a series of extensive experimental campaigns (e.g. [10,11]) performed decades ago testing with only petroleum-derived fuels suggested the relative significance of fuel physical properties over chemical properties due to their direct relationships with spray dynamics. Consequently, the current ASTM standard for jet fuel specification [12] rigorously evaluates fuel physical properties (e.g. distillation temperatures, viscosity, density), whereas only a few properties (e.g. net heat of combustion,

E-mail address: sanghee@mailbox.sc.edu (S.H. Won).

smoke point) are considered to describe fuel chemical properties. Compared to petroleum-derived jet fuels that have relatively small variations in chemical properties, recently emerging alternative jet fuels exhibit considerable variations in their chemical properties, depending on their feedstocks and synthesis approaches [13]. Recent experimental studies [13–18] suggest that fuel chemical properties cannot be overlooked for lean blow-out (LBO) conditions.

Contradictory to the historical approach that evaluates fuel chemical and physical properties separately, the potential impacts of preferential vaporization typical of multi-component real jet fuels have recently garnered an interest particularly for a near-limit combustion behavior, LBO [14]. Real liquid fuels are composed of numerous chemical components that span a wide range of molecular weights, and therefore, the fuels exhibit a relatively large difference in initial and final distillation temperatures. While constant fuel chemical property over the distillation curve has been historically assumed, it has been recognized recently that the chemical properties of jet fuels can vary significantly with distillation temperature [14,19]. Several numerical investigations using rela-

<sup>\*</sup> Corresponding author at: Department of Mechanical Engineering, University of South Carolina. Columbia. SC 29208.

tively simplified configurations have indicated the potential importance of preferential vaporization [20–22]. Recently, lab-scale experiments to assess LBO behaviors in model gas turbine combustors have also highlighted the potential significance of preferential vaporization [14,23]. Nevertheless, the potential impacts of preferential vaporization on near-limit combustion behaviors requires further examination to unravel the complexity of multicomponent, multi-phase combustion.

Compared to the Rich-Burn, Quick-Quench, Lean-Burn (RQL) combustor, the Lean-Premixed Prevaporized (LPP) combustor typically incorporates a premixer (mixing tube), thus requiring a careful design to avoid flame flashback [1]. Extensive investigations have been performed to characterize the flashback behaviors (e.g. [24-29]). Five feasible flashback mechanisms are well summarized in [27] for gas-phase combustion phenomena: flashback by autoignition, flashback in boundary layers, turbulent flame propagation in the core flow, combustion instability leading to flashback, and flashback induced by vortex breakdown. These flashback mechanisms were established at given gas phase fuel compositions without involving spray dynamics. However, for partially vaporized fuel/air mixtures, little consideration has been given to how fuel physical/chemical properties might combine to affect local chemical kinetic reactivities other than local equivalence ratio determination.

The objective of this study is to investigate and evaluate the relative significance of preferential vaporization on flame flashback relevant to multi-component fuels. A spray burner is developed, including a movable fuel injector to control the extent of fuel vaporization. To evaluate the relative significance of preferential vaporization, two different mixtures, which share the same chemical functional group distributions but have different chemical reactivity potentials during their evaporation, are formulated and tested in the spray burner. At the near-fully vaporized conditions achieved by setting the burner temperature at 700 K, the flame flashback behaviors are investigated first to ensure that the formulated two mixtures share the same chemical kinetic reactivity. Two distinct flashback modes, propagation- and autoignition-driven flashback, which are related primarily to chemical reactivity, are then examined for the two fully pre-vaporized cases.

By setting the burner temperature at 450 K to achieve partially vaporized conditions, the impact of preferential vaporization on flame flashback are examined at two different global equivalence ratios. To fruitfully evaluate the preferential vaporization impact, size, velocity, and sampling rate of droplets in fuel spray are simultaneously analyzed using Phase Doppler Particle Analyzer (PDPA), allowing the characterization of effective equivalence ratio and local flow velocity fluctuations on the partially vaporized conditions. Finally, the relative significance of preferential vaporization is discussed in terms of local laminar flame speeds based on effective equivalence ratios and local flow velocity fluctuation that affect the overall burning rates. These characteristics are examined through a Markstein number analysis based upon planar laser-induced fluorescence (PLIF) imaging.

# 2. Experimental methodology

To investigate the impact of fuel vaporization on flame flash-back characteristics, a spray burner has been developed, which can control the extent of liquid fuel evaporation. The experimental configuration is schematically illustrated in Fig. 1. To obtain a top-hat velocity profile at the exit of the nozzle, a converging section reducing the internal diameter from 50 mm to 20 mm with 75 mm in length is located. The nozzle diameter is 20 mm. Air is supplied from the bottom of the burner after passing through the electric heater, which is controlled by a PID controller to keep the air tem-

perature constant. The entire burner is heated by an electric band heater, which is also controlled through a PID controller by measuring the temperature with K-type thermocouples at three locations as indicated in Fig. 1a.

To achieve a reliable spray pattern, an air-blast spray injector was built, as described schematically in Fig. 1c. Liquid fuel is injected through a central nozzle (0.254 mm inner diameter) surrounded a coaxial outer tube with an exit inner diameter of 0.56 mm. The airflow introduced into the air-blast spray injector through the outer tube is maintained constant at 0.6 L/min throughout all measurements to minimize the changes in spray pattern. To avoid fuel vaporization inside the fuel injector and the potential change of physical properties of the liquid fuel (e.g. cavitation), cooling water is circulated inside the injector body to maintain the liquid fuel temperature at 300 K. The entire body of the air-blast spray injector is surrounded by a honeycomb structure to ensure heated airflow uniformity entering the burner. Above the honeycomb structure, a converging-diverging section (150 mm in length and 20 mm throat diameter) is located to produce uniform spray/droplet distribution characteristics. The entire injector body (including the honeycomb structure and the converging-diverging section) is designed to be moved vertically. Thus, the flow residence time inside the burner can be controlled to vary the extent of fuel spray vaporization. Here, the flow residence time is defined by the volume of the vaporization section and the volumetric flow rate of fuel and air mixture.

Airflow rates are controlled by mass flow controllers (Brooks Instrument, SLA5850) and sonic nozzles calibrated with a DryCal 800 (Mesa Labs) at room temperature. Liquid fuel is delivered by a high-pressure syringe pump (Harvard Apparatus, PHD 2000). The reported volumetric flow rate refers to the sum of fully vaporized fuel and air volumetric flow rates. Since the fraction attributed to the liquid fuel flow rate is smaller than 2% of the total flow rate (for the equivalence ratio conditions tested here), the partially vaporized conditions can be reasonably well estimated within the uncertainties of flow controllers used regardless of the extent of liquid fuel vaporization.

Direct images of premixed Bunsen flames are taken with a digital camera (Nikon, D3400). To monitor the dynamics of ignitiondriven flashback behavior, a series of Schlieren images using a LED light source (Thorlabs, M530L3) is taken with a high-speed camera (Photron, SA-Z). Flame structures as a function of the extent of fuel vaporization are also monitored by employing planar laser-induced fluorescence (PLIF) imagining for OH radical. A frequency-doubled Nd:YAG laser (Spectra-Physics, Quanta-Ray Pro-250-10) pumps a Dye laser (Spectra-Physics, Cobra-Stretch) with Rhodamine 590 to generate the excitation frequency for the  $Q_1(6)$ OH transition (~283 nm, 6 mJ/pulse). The beam is spread and focused into a sheet ( $\sim$  150  $\mu m$  thick and  $\sim$  60 mm tall) by using a cylindrical lens and a plano-convex lens and directed across the center of the burner. The fluorescence image is captured by an Intensified CMOS camera (Andor, iStar sCMOS) with a 100 mm f/2.8 UV lens (Cerco) and two bandpass filters (UG-11 and WG-305).

To characterize the spray properties, the droplet size and velocity distributions are measured using a Phase Doppler Particle Analyzer (PDPA, TSI). A single component fuel, n-dodecane (nC12) supplied at a global equivalence ratio of unity, was used to test partial vaporization operation at a burner temperature of 400 K. The spray burner developed is an adaptation of the design concept reported in [30,31], developed to achieve near-homogenous droplet and velocity distributions at the nozzle exit. To confirm these behaviors, droplet size and velocity distributions were measured radially by PDPA at 3 mm above the nozzle exit. Fig. 2a shows the radial distributions of the arithmetic mean diameter  $(d_{10})$ , surface mean diameter  $(d_{20})$ , and volume mean diameter  $(d_{30})$  at the mean

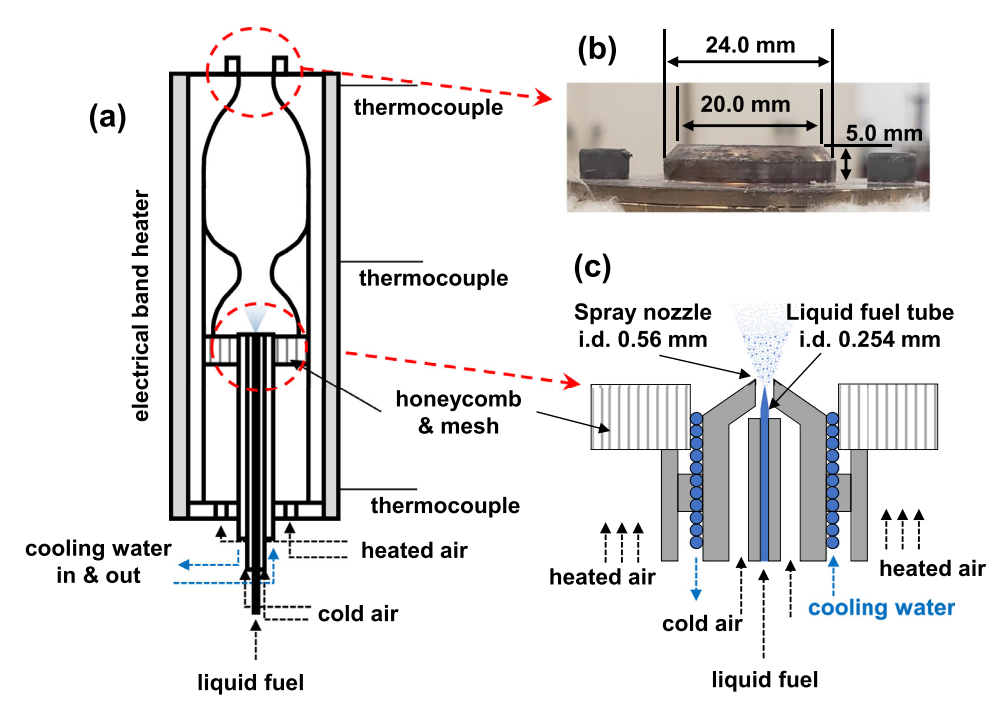
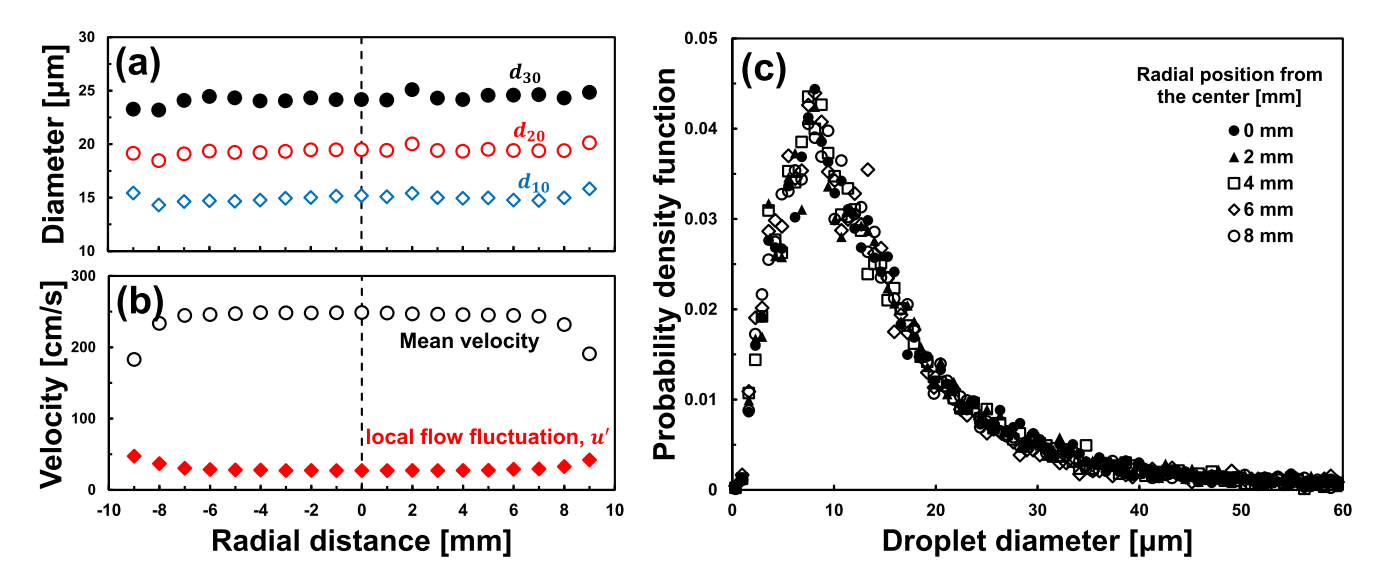


Fig. 1. (a) Schematics of spray burner, (b) direct photo at the nozzle exit, and (c) schematics of movable spray injector.



**Fig. 2.** (a) Radial distributions for three droplet sizes, arithmetic mean diameter ( $d_{10}$ ), surface mean diameter ( $d_{20}$ ), and volume mean diameter ( $d_{30}$ ) measued by PDPA at  $U_0 = 240$  cm/s for stoichiometric n-dodecane/air mixture at 400 K. (b) Radial profiles of the mean velocity and local velocity fluctuation (u') defined from standard deviation measured by PDPA. (c) Distributions of droplet diameters for various radial positions at 3 mm above nozzle exit.

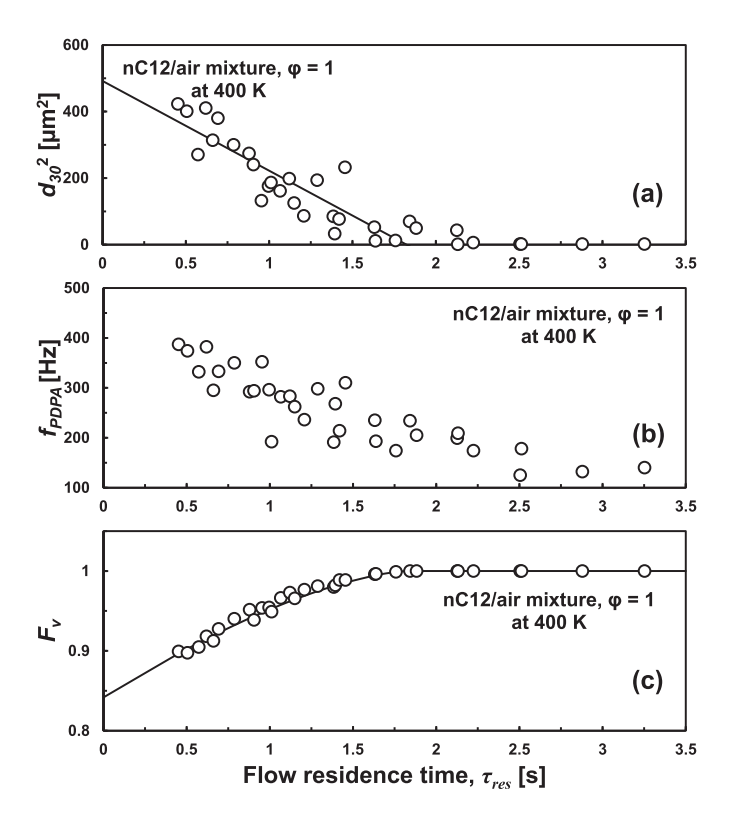
jet velocity ( $U_0$ ) of 240 cm/s. Fig. 2**b** depicts the radial profiles of the mean velocity and local velocity fluctuation (u') determined from the standard deviations of the PDPA measurements. The measured mean velocities by PDPA agree with the mean jet velocity based on volumetric flow rate within 2% uncertainty. Considering the Stokes number calculated based on the measured droplet diameter and burner nozzle diameter is < 0.1, the velocity measurements by PDPA can be reasonably regarded as the flow velocity and its fluctuation [32].

Fig. 2c shows the measured droplet size distribution at various radial positions, exhibiting near-identical characteristics regardless radial position. Near-constant values of  $d_{10}$ ,  $d_{20}$ , and  $d_{30}$  in Fig. 2a and near-identical droplet size distribution along the radial direction suggest that droplet size distributions are uniform, assuring

that measurements at the center of the nozzle flow are accurate representations of the spray characteristics.

Subsequently, the droplet size distributions with changing flow residence time (extent of vaporization) are characterized by PDPA measurements at the center of the burner exit. Flow residence time ( $\tau_{res}$ ) is controlled by changing fuel and airflow rates, as well as moving the injector location. Here, we use volume mean diameter ( $d_{30}$ ) instead Sauter mean diameter ( $d_{32}$ ), to properly evaluate the extent of fuel vaporization based on volumetric fuel flow rates.

Fig.  $3\mathbf{a}$  shows the squared values of the measured  $d_{30}$  as a function of  $\tau_{res}$ . In the case of fuel vaporization in spray, the rate of fuel vaporization is known to be governed through the complicated interactions among the spray droplets [33,34]. Nevertheless, the theoretical analyses suggest that the rate of fuel droplet vaporization



**Fig. 3.** Summary of PDPA measurements at the nozzle exit for stoichiometric n-dodecane/air mixture at 400 K as a function of flow residence time  $(\tau_{res})$ ; (a) the squared values of the measured  $d_{30}$  as a function of  $\tau_{res}$ , (b) the measured PDPA sampling frequency  $(f_{PDPA})$  as a function of  $\tau_{res}$ , and (c) the calculated vaporized fuel fraction as a function of  $\tau_{res}$ .

follows the typical  $D^2$  law for a single droplet, once the distances between the droplets are sufficiently large [33,34]. Based on the volumetric flow rate and the measured  $d_{30}$  as well as the sampling frequency of PDPA measurement ( $f_{PDPA}$ ), the mean distance among fuel droplets are estimated ten times larger than  $d_{30}$  (>  $10d_{30}$ ), supporting the observed moderate linear trend of  $d_{30}^2$  as a function of  $\tau_{res}$ . When  $\tau_{res} > 3$  s, the measured  $d_{30}$  becomes smaller than 2 µm, comparable to the PDPA measurement limit ( $\sim 1$  µm), indicative of reaching a fully vaporized condition.

The increased extent of fuel vaporization with  $\tau_{res}$  can be also seen from the sampling frequency in PDPA measurements ( $f_{PDPA}$ ), as shown in Fig. 3b, which monotonically decreases as increasing  $\tau_{res}$ . The volume fraction of fuel vaporized ( $F_{v}$ ) can be determined by incorporating the measured  $d_{30}$  and  $f_{PDPA}$  in the following equation.

$$F_v = 1 - \frac{\pi d_{30}^3}{6Q_{fuel}} \frac{A_{nozzle}}{A_{PDPA}} f_{PDPA}$$
 (1)

Here,  $A_{nozzle}$  and  $A_{PDPA}$  are the area of the burner exit and the cross-sectional area of the sampling volume of the PDPA, respectively. Here,  $A_{nozzle}$  is calculated based on the nozzle diameter and  $A_{PDPA}$  is estimated based on the laser beam alignment as described in the TSI operations manual. The two identical laser beams from the PDPA cross at the measurement volume bounded by the ellipsoidal surface, which is the surface that the light intensity of fringe is  $1/e^2$  of the maximum intensity. With the given half-angle  $(\theta)$  between two laser beams and laser diameter  $(D_{e^{-2}})$ ,  $A_{PDPA}$  is  $4f^2\lambda^2/\pi D_{e^{-2}}^2\sin\theta$ . Here, f and  $\lambda$  are the focal length of the lens in PDPA and laser wavelength, respectively.  $Q_{fuel}$  is total fuel flow rate into the spray burner.

**Table 1**Summary of two binary component mixtures formulated by matching key chemical functional group distribution.

	Mixture 1 (nC8/iC16)	Mixture 2 (iC8/nC16)
n-octane (nC8)	0.74	0
iso-octane (iC8)	0	0.67
n-hexadecane (nC16)	0	0.33
iso-cetane (iC16)	0.26	0
Calculated DCN	53.4	53.6
(CH <sub>2</sub> ) <sub>n</sub> /CH <sub>3</sub> molar ratio	1.16	1.15

Fig. 3c shows the estimated volume fraction of fuel vaporized  $(F_v)$  as a function of  $\tau_{res}$ . The solid line is derived from fitting into the following equation by varying  $d_{30.initial}$ .

$$F_{\nu} = 1 - \left(\frac{d_{30}}{d_{30, initial}}\right)^{3} \tag{2}$$

The initial  $d_{30}$  values ( $d_{30,\,initial}$ ) estimated from Eq. (2) is 41 µm, which is different from the estimation from the linear extrapolation on the observed moderate linear trend of  $d_{30}^2$  ( $\sim$ 24 µm). This difference can be attributed to the existence of the converging-diverging section to achieve uniform distribution of spray droplets inducing local flow acceleration, therefore reducing the dynamic pressure resulting in accelerating the fuel vaporization. Nevertheless, the results shown in Fig. 3 confirm that the extent of fuel vaporization can be controlled by changing the mean flow rate and/or the injector location that governs the flow residence time.

#### 3. Formulation of binary component test mixtures

Combustion behaviors of partially vaporized fuel/air mixtures inevitably involve complicated coupling impacts between fuel physical and chemical properties. Recent experimental observations of lean blow-out (LBO) with petroleum-derived jet fuels, alternative jet fuels, and their blends suggest that the impact of fuel chemical property may also be significant [14–17]. The significant role of fuel chemical property appeared through a strong correlation of LBO with the derived cetane number (DCN) of fuel that represents the chemical reactivity potential [13, 35–37].

Knowing that the impact of preferential vaporization on nearlimit combustion behaviors appears through complicated interactions, two binary component mixtures were specifically formulated based on our previous works [35, 37-42] to simplify the analysis. Mixture 1 is composed of n-octane (nC8) and iso-cetane (iC16) and Mixture 2 is composed of iso-octane (iC8) and n-hexadecane (nC16), as summarized in Table 1. The mixture compositions were optimized to achieve a similar DCN value of n-heptane (53.8), thus exhibiting a similar chemical reactivity potential. In the case of nalkane/iso-alkane mixtures, the overall chemical kinetic characteristics of these fuels are primarily governed by the ratio of methylene (CH<sub>2</sub>) and methyl (CH<sub>3</sub>) functionalities [37]. The relative contributions of CH<sub>2</sub> and CH<sub>3</sub> functionalities on global combustion behaviors were further contrasted by introducing a methylene chain,  $(CH_2)_n$   $(n \ge 3)$ , which not only governs the low-temperature chain branching reactions but also reflects high-temperature reactivities, as discussed in [35,38]. The two mixtures also share very similar values of the (CH<sub>2</sub>)<sub>n</sub> to CH<sub>3</sub> molar ratio, therefore it is expected to exhibit identical chemical kinetic reactivities in both high- and low-temperature combustion regimes.

Though these two binary component mixtures have identical global combustion behaviors for fully vaporized conditions, their combustion behaviors are expected to differ when preferential vaporization is important. To evaluate this difference, the fuel boiling temperatures and local gas-phase compositions are calculated

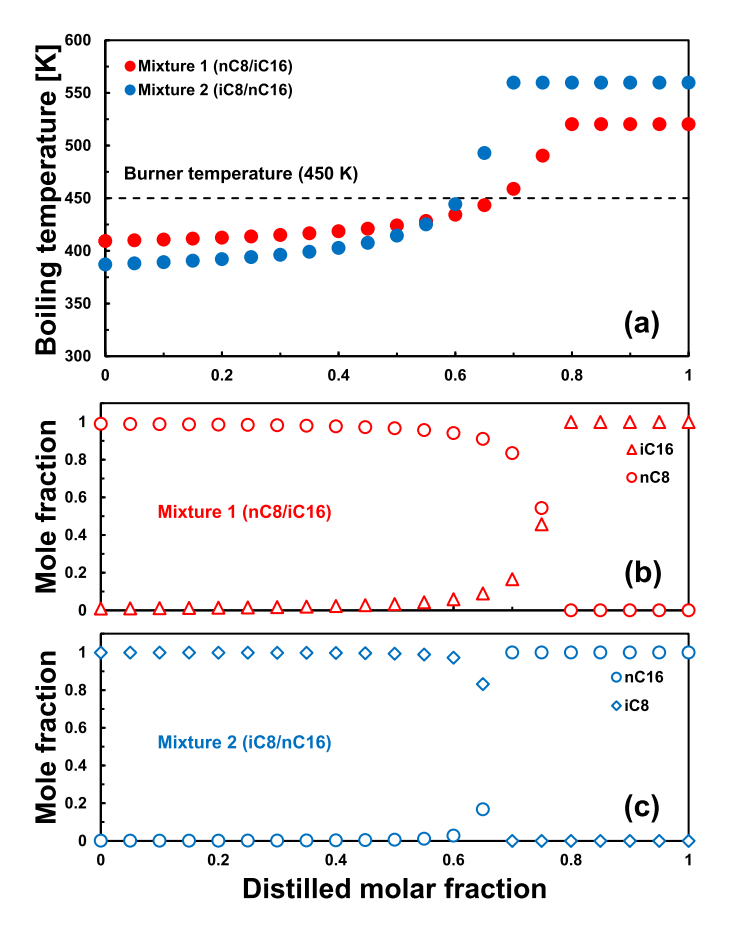


**Fig. 4.** (a) Boiling temperatures for two binary component mixtures with distilled molar fraction, (b) mole fractions of nC8 and iC16 with distilled molar fraction for Mixture 1, and (c) mole fractions of iC8 and nC16 with distilled molar fraction for Mixture 2.

as a function of distilled molar fraction as shown in Fig. 4. The approach to calculate the fuel distillation curve can be found in [35,43]. Although the two mixtures are formulated with the same carbon numbers (C8 and C16), the difference in boiling temperatures between nC8 and iC8 results in a slightly higher initial boiling temperature for Mixture 1 due to the slightly higher boiling temperature of nC8 over iC8 (Fig. 4a). Similarly, due to the lower boiling temperature of iC16 than that of nC16, the final boiling temperature of Mixture 1 is slightly lower than that of Mixture 2.

Fuel composition in gas phase from vaporizing mixtures changes over fuel vaporization process due to the difference in the boiling temperature between the components in the mixtures. In the case of Mixture 1 shown in Fig. 4b, the lighter component nC8 evaporates earlier than the heavier component iC16, thus depositing a relatively reactive component in the gas phase. However, iC8 evaporates earlier in the case of Mixture 2 (Fig. 4c), which has lower chemical reactivity compared to nC8 in Mixture 1. Therefore, it is expected that Mixture 1 will have a higher reactivity (e.g. laminar flame speed, ignition propensity) than Mixture 2 when the preferential vaporization occurs.

#### 4. Results and discussion

#### 4.1. Flame flashback behaviors in fully vaporized condition

Prior to the experiments for partially vaporized conditions, the flame flashback behaviors in the fully vaporized conditions are investigated by setting the burner temperature at 700 K. To determine flame flashback conditions, a stable flame at relatively higher

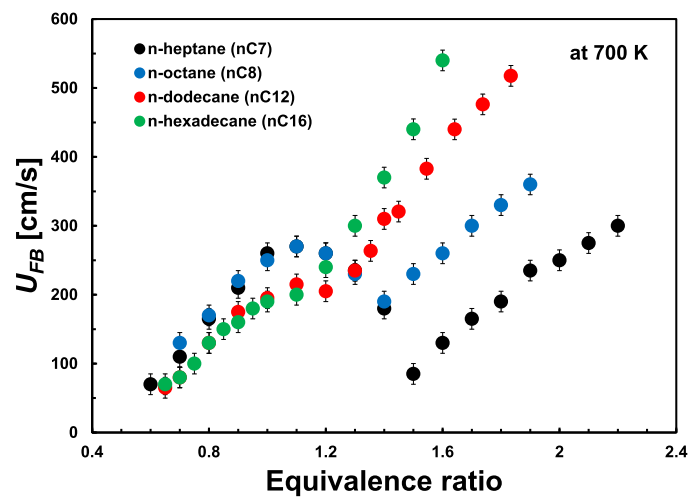


**Fig. 5.** Measured  $U_{FB}$  as a function of global equivalence ratio  $(\varphi_g)$  for four n-alkanes, n-heptane (nC7), n-octane (nC8), n-dodecane (nC12), and n-hexadecane (nC16) at 700 K (fully vaporized condition).

mean jet velocity is firstly established at the exit of the nozzle. Then, the mean jet velocity is gradually reduced until the flame base suddenly penetrates inside the burner. When flame flashback occurs, the mean jet velocity  $(U_0)$  is assigned as  $U_{FB}$ . Fig. 5 shows the measured  $U_{FB}$  as a function of global equivalence ratio  $(\varphi_g)$ for four n-alkanes, n-heptane (nC7), n-octane (nC8), n-dodecane (nC12), and n-hexadecane (nC16). As clearly depicted in Fig. 5, there are two distinct regimes for n-alkanes, propagation-driven flashback at relatively lean equivalence ratios and ignition-driven flashback at relatively rich equivalence ratios. Those two different flashback modes are distinguished by observing how the flashback occurs. When the burning rate of flame is faster than volumetric flow rate of gas mixture, the propagation-driven flashback occurs by the flame propagating back to the inside of the burner. On the other hand, the ignition-driven flashback happens with the autoignition of mixture, creating the flame inside the burner.

While the propagation-driven flashback is primarily controlled by laminar flame speed and diffusive characteristics [44,45], the ignition-driven flashback is controlled by the onset of autoignition as discussed previously elsewhere [46,47]. The onset global equivalence ratios of n-alkanes become leaner as increasing the molecular weight of n-alkane (the length of CH<sub>2</sub> backbone), 1.5 for nC7, 1.4 for nC8, 1.3 for nC12, and 1.2 for nC16, inversely proportional to their DCN values [48]. Since the flow residence time ( $\tau_{res}$ ) inside the burner is inversely proportional to  $U_{FB}$ , the results suggest that the autoignition delay time becomes shorter as the chain length of the CH<sub>2</sub> backbone in n-alkanes is increased. This trend is qualitatively identical to the predicted and measured dependency of homogenous reflected shock ignition delay times in terms of n-alkane chain length and equivalence ratio [2,37, 49-52].

Fig. 6 shows the time series of Schlieren images for n-dodecane at the global equivalence ratio,  $\varphi_g=1.4$ ,  $U_0=280$  cm/s. Initially (at t=0 ms), the Schlieren image clearly shows a typical Bunsen premixed flame attached to the nozzle exit represented by a sharp density gradient. Similar to the previous work [47], the autoignition kernel appears at the nozzle exit at 0.25 ms, indicating that autoignition occurs at the given flow residence time, thus inducing the ignition-driven flashback. The autoignition kernel continues to grow and merges with the premixed flame at  $\sim$  1.25 ms. Then, the entire flame starts penetrating into the burner inside, eventually completing the flashback sequence at  $\sim$  2.25 ms, where no discernible flame structure can be seen.

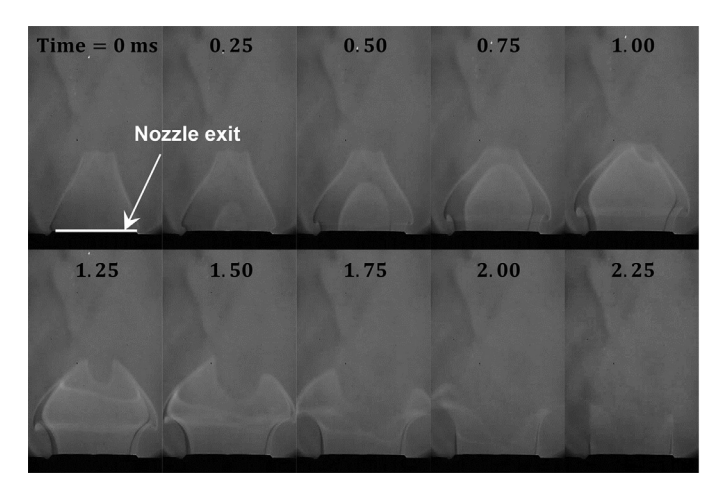


**Fig. 6.** Time series of Schlieren images for n-dodecane at the global equivalence ratio,  $\varphi_{\rm g}=1.4$ , and  $U_0=280$  cm/s for ignition-driven flashback behaviors. Nozzle exit is marked with a white line.

The transitions to ignition-driven from propagation-driven flashbacks in Fig. 5 are demarcated clearly for nC7 and nC8, while those of nC12 and nC16 are found to occur smoothly as a function of  $\varphi_g$ . These results can be attributed to the mechanistic behaviors of the two-stage ignition process in low-temperature conditions. Both the first- and second-stage ignition delay times become shorter with increasing the length of CH<sub>2</sub> backbone in nalkanes and the interval between the first- and second-ignition delay times also become shorter with increasing equivalence ratio [52-54]. Thus, the fast transition to the second-stage ignition at rich conditions renders more abrupt and distinct transition to the ignition-driven flashback for nC7 and nC8. Relatively smooth transitions found for nC12 and nC16 can be attributed to the excessive heat release after the first-stage ignition that affects the transition to the second-stage ignition. Although not specifically measured during the experiments, the temperature measurement at the nozzle exit exhibits a continuous increase approaching ~ 80 K over the setpoint (700 K), coinciding with the onset of ignition-driven flashback. Heat loss occurs inside the burner after the onset of the first-stage ignition, thus lowering the global burning rate and the measured  $U_{FR}$ , compared to nC7 and nC8. Chemical kinetic characteristics associated with heat loss after the first-stage ignition have been discussed previously in [47], and further characterization and discussion here is beyond the scope of the present investigation.

Fig. 7 compares the measured  $U_{FB}$  values of two binary component mixtures at fully vaporized condition with 700 K of the burner temperature. Within measurement uncertainty, the two mixtures exhibit almost identical flashback behaviors for both propagation- and ignition-driven flashback regimes. This result confirms the effectiveness of the mixture formulation by matching the key chemical functional group distributions as shown in Table 1. It suggests that the flashback behaviors of the two mixtures will be similar at the near-fully vaporized conditions. It also implies that results will differ under preferentially vaporizing conditions due to the difference of laminar flame speed caused by the composition difference shown in Fig. 4, which governs the propagation-driven flashback behaviors [24–29].

#### 4.2. Flame flashback behaviors in partially vaporized condition

Confirming the commonality of flashback behaviors of two binary component mixtures once they are fully vaporized, the potential impacts of preferential vaporization on flame flashback are investigated at a partially vaporized condition. The burner temper-

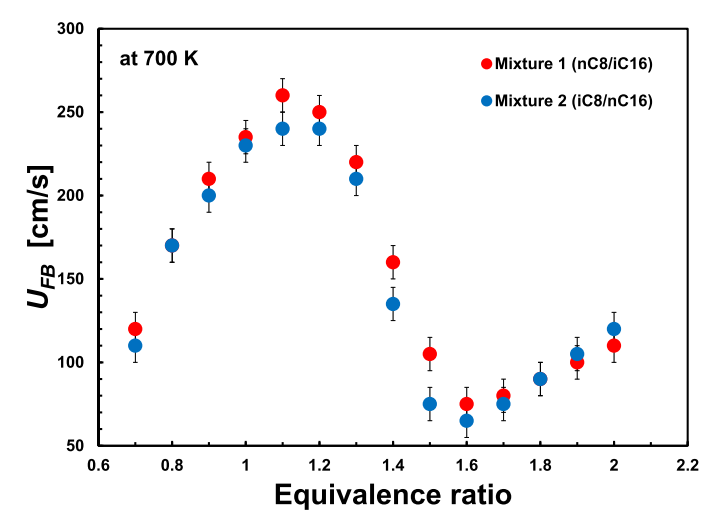


**Fig. 7.** Comparison of the measured  $U_{FB}$  values for two binary component mixtures at fully vaporized condition at 700 K burner temperature as a function of equivalence ratio.

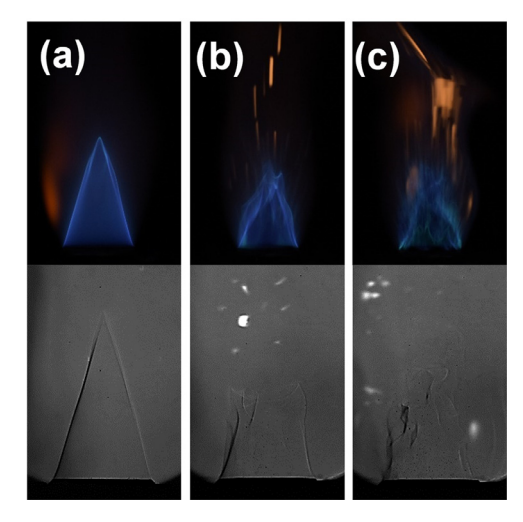


**Fig. 8.** Direct photos (top) and Schlieren images (bottom) of n-dodecane flames at  $\varphi_g=1$  and  $U_0=280$  cm/s by varying the flow residence time ( $\tau_{res}$ ) at 450 K. (a)  $\tau_{res}=1.22$  s, (b)  $\tau_{res}=0.54$  s, and (c)  $\tau_{res}=0.32$  s.

ature is reduced from 700 K to 450 K based on the calculated distillation behaviors of two mixtures as shown in Fig. 4.

Before testing the binary component mixtures, flame behaviors as a function of flow residence time were observed for ndodecane. Fig. 8 shows direct photos (top) and Schlieren images (bottom) of n-dodecane flames at  $\phi_g=1$  and  $U_0=280$  cm/s by varying the flow residence time ( $\tau_{res}$ ) at various injector positions. At  $\tau_{res} = 1.22$  s, a stable Bunsen premixed flame can be observed (Fig. 8a), indicating that  $\tau_{res}$  is long enough to fully evaporate the atomized liquid n-dodecane spray inside the burner. By reducing  $\tau_{res}$  to 0.54 s (Fig. 8b), an unstable Bunsen premixed flame was observed. As the extent of fuel vaporization is further reduced by shortening  $\tau_{res}$  to 0.32 s, the flame structure is significantly perturbed as shown in Fig. 8c. The perturbation of flame structures at the partially vaporized conditions can be attributed primarily to the local flow velocity fluctuation that has a strong correlation with the extent of fuel vaporization (shown in Figs. 9d and 10d). Instantaneous vaporization of fuel droplets near the flame surface induces convective flow perturbation through the interaction between Stefan flow and the density difference during the phase change [55,56]. Further details are discussed later with PLIF images.

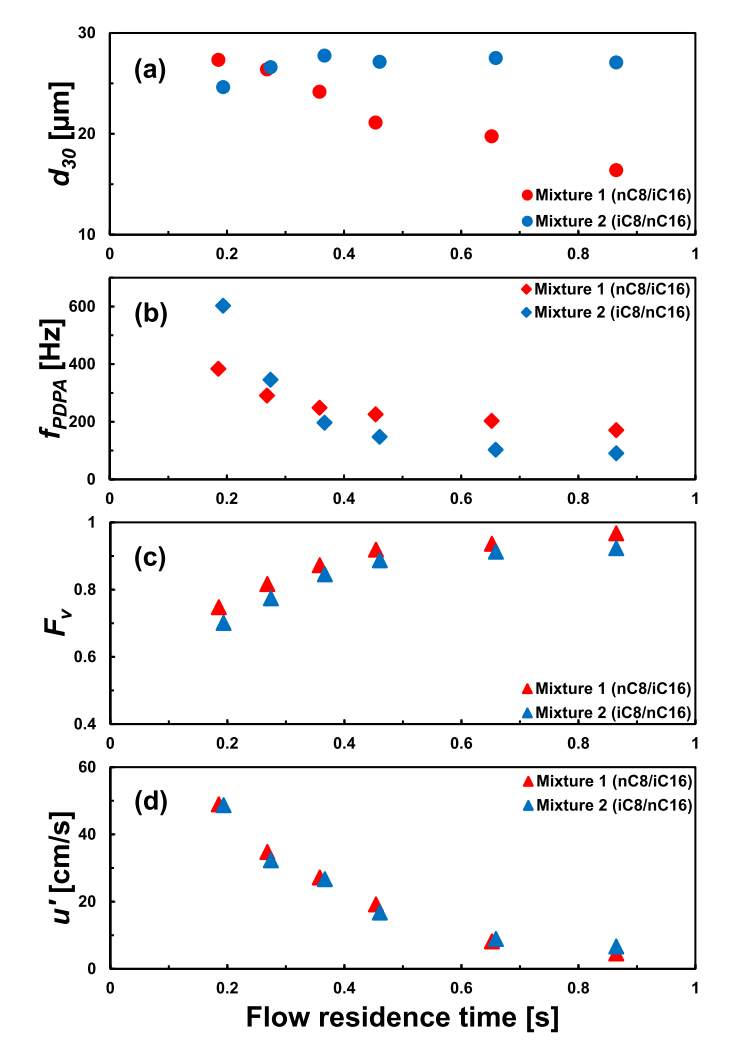


**Fig. 9.** Summary of PDPA measurements for two mixtures at  $\varphi_g = 1.0$  as a function of  $\tau_{res}$  at 450 K; (a) the measured  $d_{30}$  values, (b) the measured PDPA sampling frequency  $(f_{PDPA})$ , (c) the calculated vaporized fuel fraction (Fv), and (d) local velocity fluctuation (H').

To further elaborate upon the role(s) of preferential vaporization on flame flashback behaviors, the images shown in Fig. 8 suggest that two other impacts should be considered carefully. First, it is necessary to determine the extent of fuel vaporization, which defines the deposition of gas phase fuel before the flame front. When the injected liquid droplets are partially vaporized, the vaporized fuel mixed with air determines the effective equivalence ratio, which would control the overall burning rate of flames, therefore the onset of flashback. The other is the influence of local velocity perturbation caused by the instantaneous vaporization of fuel droplets when the fuel droplets before/after entering the flame preheat zone. The local flow velocity perturbation results in wrinkling of the flame structure, increasing the overall burning rate by increasing the effective flame surface area. To quantify and evaluate the contributions from these two physics, spray properties were systematically measured by PDPA at 3 mm above the nozzle exit, which determines the droplet diameter  $(d_{30})$  and the local flow perturbation (u') simultaneously.

Fig. 9a shows the measured  $d_{30}$  values for both binary component mixtures at the global equivalence ratio of 1.0 ( $\varphi_g=1.0$ ) as a function of flow residence time ( $\tau_{\rm res}$ ). While the measured  $d_{30}$  values of Mixture 1 exhibit a monotonically decreasing trend, those of Mixture 2 exhibit relatively constant values. This can be attributed to the difference in boiling temperatures between nC16 and iC16,

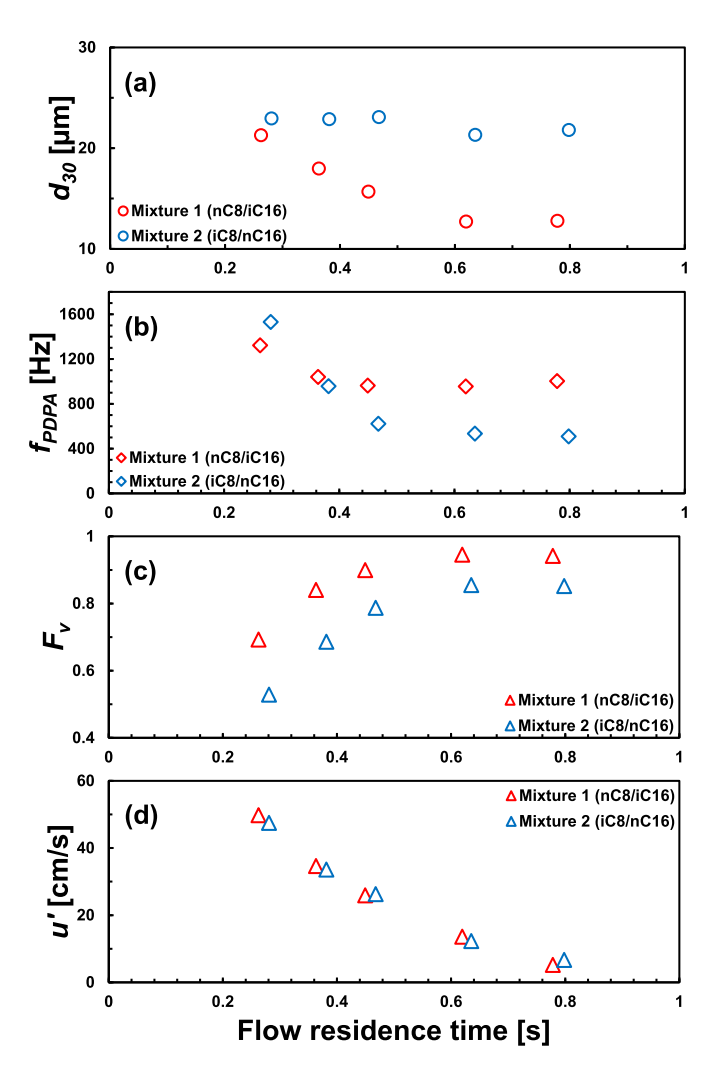


**Fig. 10.** Summary of PDPA measurements for two mixtures at  $\varphi_g = 1.4$  as a function of  $\tau_{res}$  at 450 K; (a) the measured  $d_{30}$  values, (b) the measured PDPA sampling frequency  $(f_{PDPA})$ , (c) the calculated vaporized fuel fraction (Fv), and (d) local velocity fluctuation (u').

which are 554 K and 513 K, respectively. Although the measured  $d_{30}$  values for Mixture 2 do not change much, the measured PDPA frequency ( $f_{PDPA}$ ) decreases considerably with  $\tau_{res}$ , suggesting that the lighter component in Mixture 2 (iC8) continuously evaporates from the fuel droplets. Combining the results in Figs. 9a and b, the extent of fuel vaporization can be estimated by using Eq. (1).

Fig. 9c shows the vaporized fraction  $(F_v)$  as a function of  $\tau_{res}$ , demonstrating that the extent of fuel vaporization increases as increasing  $\tau_{res}$ . The estimated  $F_v$  value allows calculating the effective equivalence ratio ( $\varphi_{effective}$ ). The calculated  $\varphi_{effective}$  of Mixture 1 varies from 0.73 to 0.97 with increasing  $\tau_{res}$ , and from 0.68 to 0.92 with Mixture 2. To evaluate the local flow velocity perturbations, the standard deviations of the measured droplet velocities by PDPA are shown in Fig. 9d. The average values of droplet velocities (not shown) coincided with the mean jet velocities to within measurement uncertainties (< 5%).

Fig. 10 summarizes the results of PDPA measurements for the two mixtures at  $\varphi_g=1.4$ . The estimated vaporized fraction in Fig. 10**c** shows that Mixture 1 approaches the near-fully vaporized condition at large  $\tau_{res}$ , whereas Mixture 2 does not achieve a fully vaporized condition in the range of  $\tau_{res}$  investigated in this study. Accordingly, the calculated  $\varphi_{effective}$  varies with increasing  $\tau_{res}$  from 0.94 to 1.32 for Mixture 1 and from 0.70 to 1.18 for Mixture 2.

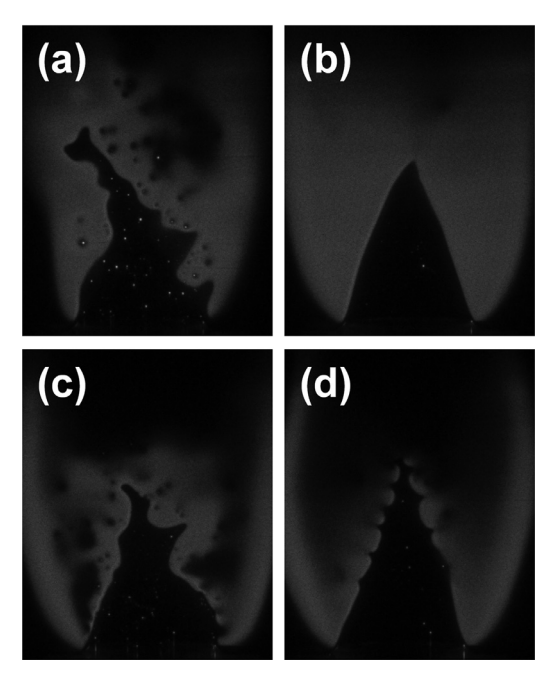


**Fig. 11.** Representative OH PLIF images at 450 K; (a) Mixture 1 at  $\varphi_g=1.0$  and  $\tau_{res}=0.22$  s, (b) Mixture 1 at  $\varphi_g=1.0$  and  $\tau_{res}=0.70$  s, (c) Mixture 2 at  $\varphi_g=1.4$  and  $\tau_{res}=0.22$  s, and (d) Mixture 2 at  $\varphi_g=1.4$  and  $\tau_{res}=0.70$  s.

The changes of the effective surface burning area due to the local flow perturbation from droplet vaporization were evaluated by taking OH PLIF images of two mixtures as a function of  $\tau_{res}$ by adjusting the fuel injector location at the fixed  $U_0 = 280$  cm/s. In general, no considerable differences in flame surface wrinkling were observed between Mixture 1 and Mixture 2, regardless of  $\varphi_g$ and  $\tau_{res}$ . Fig. 11**a** and **b** show the flame structures of Mixture 1 for  $\varphi_g = 1.0$  at  $\tau_{res} = 0.22$  s and 0.70 s, respectively. Compared to the near-fully vaporized condition at  $\tau_{res} = 0.70$  s, which exhibits a typical premixed Bunsen flame, the OH PLIF image at  $\tau_{res} = 0.22$  s clearly shows pronounced flame surface wrinkling. Multiple local regions having no OH LIF signals are observed just downstream of the flame surface, which are induced by the instantaneous evaporation of fuel droplets as they pass through the flame surface. In the case of  $\varphi_g=1.4$ , the OH PLIF image at  $\tau_{res}=0.22$  s in Fig. 11c also shows pronounced flame surface wrinkling similar to that in

A strong inverse proportionality of u' with  $\tau_{res}$  (and the extent of fuel vaporization,  $F_{\nu}$ ) for both global equivalence ratio conditions suggests that the local flow velocity perturbations are caused by instantaneous droplet evaporation. Instantaneous droplet evaporation induces local flow perturbation through the interaction between Stefan flow and the density difference during the phase change [55,56]. The time interval of flow from the nozzle exit to the flame surface is estimated as  $\sim$  10 ms for the conditions tested. Based on the extent of fuel vaporization shown in Figs. 9c and 10c, the resultant change of effective equivalence ratio due to the continuous fuel droplet evaporation between nozzle exit and flame surface is estimated to be < 0.01 for the worst case, suggesting indiscernible variations of effective equivalence ratio. Furthermore, the convective time scale for mixing induced by flow perturbation can be estimated O(1 ms) with u' and the average interval between droplets ( $\sim 10d_{30}$ ) at  $\tau_{res} \sim 0.2$ , suggesting relatively strong mixing prior the flame surface.

When a small fuel droplet penetrates through the premixed flame preheat zone, it might be immediately vaporized, thus forming either a locally fuel-rich condition or a diffusion flame. Each phenomenon can result in potential acceleration of flame propagation due to the local mixture fraction gradient [57–59]. To address this possibility, the effective burning area defined by flame surface perimeters were evaluated from 50 images of OH PLIF by varying  $\tau_{res}$ . Although not shown in the figure, the effective burning area exhibits a monotonically increasing trend with u', but with no apparent relation to  $d_{30}$ . Nevertheless, the OH PLIF images in Figs. 11a and 11c show locally perturbed flame curvature associated with droplet evaporation and/or formation of diffusion flame. However, the OH LIF intensities along the wrinkled flame surface exhibits indiscernible changes, thus their contributions to the overall burning rate can be assumed to be minimal. Consequently, the vaporized fuel/air mixture can be considered to be spatially uniform, allowing the evaluation of its laminar flame speed based on the effective equivalence ratio derived from the extent of fuel vaporization.

In the previous studies [60-62], it was reported that the existence of small fuel droplets could trigger the diffusive-thermal instability, thus potentially enhancing flame propagation. While such a flame surface instability was not observed in the partially vaporized conditions for either global equivalence ratio studied, it is found at higher extents of fuel vaporization at  $\varphi_g=1.4$ . PLIF images for Mixture 2 at  $au_{res} = 0.70$  s and  $arphi_g = 1.4$  clearly shows the flame surface characteristics typical to diffusive-thermal instability (Fig. 11d). A similar behavior was also found for Mixture 1 at  $\varphi_g = 1.4$  and near-fully vaporized conditions. In the case of a premixed Bunsen flame with gaseous fuel/air mixture, a diffusivethermal instability typically occurs when the mixture Lewis number (Le) is less than unity [63]. Considering the effective Lewis number for both mixtures at near-fully vaporized conditions is  $\sim$ 1.1, the observed flame surface instabilities could be attributed to the onset of a diffusive-thermal instability due to the existence of small fuel droplets. Further detailed characterization of the instability behavior was not pursued. Rather, the measurements exhibiting instability were excluded in the analysis below so as to focus solely on the evaluating the impact of preferential vaporization on flame flashback behaviors.

Fig. 12**a** compares the measured  $U_{FB}$  values of two mixtures as a function of  $\varphi_{effective}$  for measurements performed at  $\varphi_g=1.0$ . The two mixtures should have almost identical laminar flame speed behaviors (thus  $U_{FB}$ ) as a function of  $\varphi_{effective}$  in the absence of preferential vaporization. Thus, the observed difference in  $U_{FB}$  must be attributed to the impact of preferential vaporization. The laminar flame speed is a major governing parameter for propagationdriven flashback [24-29]. Therefore, the laminar flame speed with the preferential vaporization  $(S_{L,local})$  and that without  $(S_{L,NPV})$  (assuming no change in fuel composition) were calculated using a reduced chemical kinetic model [64]. The ratios of  $S_{L,local}$  to  $S_{L,NPV}$ as a function of the given  $\varphi_{effective}$  are plotted in Fig. 12**b**. The data shows a disparity between the two mixtures for partially vaporized (low  $\varphi_{effective}$ ) conditions, which essentially disappears as fully vaporized condition ( $\varphi_{effective} = \varphi_g = 1.0$ ) is approached. Fig. 12**c** compares  $U_{FB}$  normalized by  $S_{L,local}$  for the two mixtures, further supporting that the difference in  $S_{I,local}$  induced by preferential vaporization primarily governs the observed difference in

Fig. 13a compares the measured  $U_{FB}$  values for the two mixtures as a function of  $\varphi_{effective}$  at  $\varphi_g=1.4$ . The overall trend of the measured  $U_{FB}$  is qualitatively similar to the results found for  $\varphi_g=1.0$ , i.e., there is a relatively large difference in  $U_{FB}$  for partially vaporized conditions that essentially disappears as near-fully vaporized condition is approached, noted by considering  $S_{L,local}$  in Fig. 13b. Fig. 13c shows the  $U_{FB}$  normalized by  $S_{L,local}$ , again confirming the significance of preferential vaporization to flame flash-back behaviors.

The commonalities in  $U_{FB}$  of the two binary component mixtures found through normalization of the data by  $S_{L,local}$  for both

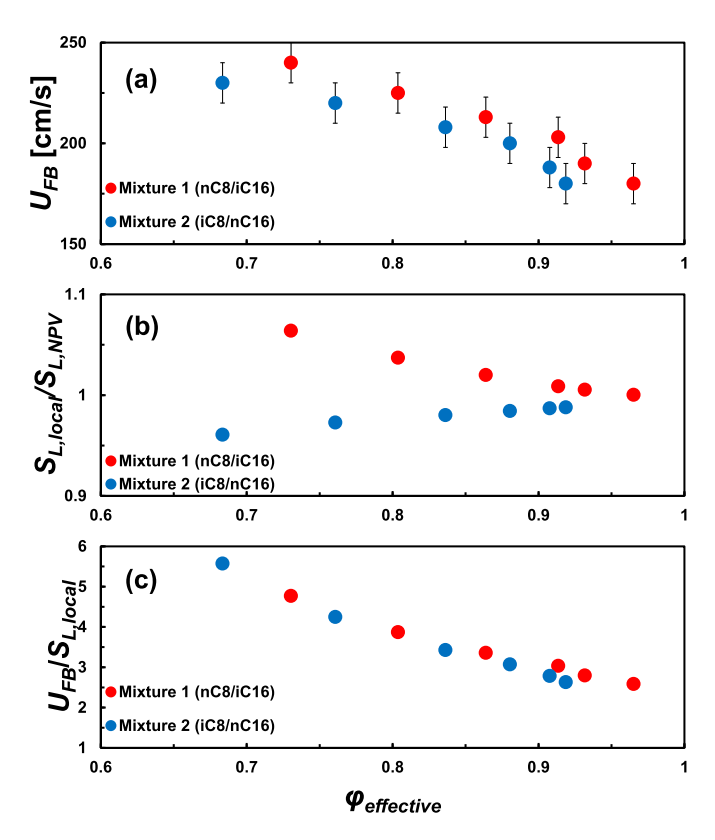


**Fig. 12.** Comparison of flashback behaviors for two mixtures with  $\varphi_{effective}$  at  $\varphi_g = 1.0$  in the partially vaporized condition (450 K); (a) the measured  $U_{FB}$  values, (b) the ratio of laminar flame speed ( $S_{L,local}$ ) considering the preferential vaporization to the one ( $S_{L,NPV}$ ) without considering the preferential vaporization, (c) the measured  $U_{FB}$  values normalized by local laminar flame speed ( $S_{L,local}$ ).

 $\varphi_g$  conditions in Figs. 12**c** and 13**c** indicate that preferential vaporization affects global burning characteristic, and hence, flame flashback behavior. Fig. 14**a** combines the results for both  $\varphi_g$  conditions as a function of  $\varphi_{effetive}$ . The result shows that the normalized  $U_{FB}$  by  $S_{L,local}$  for the fuel-lean conditions is considerably more sensitive to  $\varphi_{effetive}$  than for fuel-rich conditions, regardless of  $\varphi_g$ . Considering the Reynolds number employed in these measurements based on the nozzle diameter (1000 < Re < 1600), the premixed Bunsen flames observed here locate in the wrinkled flamelet regime of the Borghi diagram [65,66]. In these cases, thermo-diffusive effects play an important role in the overall burning rate through interactions with local flow perturbations, thus influencing the local stretch rate [67-71]. As the flames experience flow stretch due to the local fuel evaporation near the flame reaction zone, the overall burning rates are affected by both local laminar flame speed perturbations as well as by flame stretch. The Markstein number, defined as the ratio of Markstein length to flame thickness, characterizes the relative sensitivity of the overall burning rate to the flame surface topology and local flame front curvature. Markstein length (L) can be estimated for a wide range of equivalence ratios as proposed in [70], as well as by considering the effective Lewis number as suggested in [70,71]. Overall activation energy effects have been evaluated by varying nitrogen dilution of mixtures at the concentration of nitrogen in the mixtures at different equivalence ratios as described in [69].

In the wrinkled flamelet regime, the overall burning rate is affected by the local flow stretch rate  $(\kappa)$  and Markstein length (L) through  $S_{ovearll} = S_L - L\kappa$  [67–71]. Accordingly, the similar tendencies of  $U_{FB}/S_{L,local}$  in Fig. 14**a** and Markstein length (L) in Fig. 14**b** imply that the measured  $U_{FB}$  as a function of  $\varphi_{effetive}$  at fuellean conditions is more sensitive to flame stretch caused by lo-

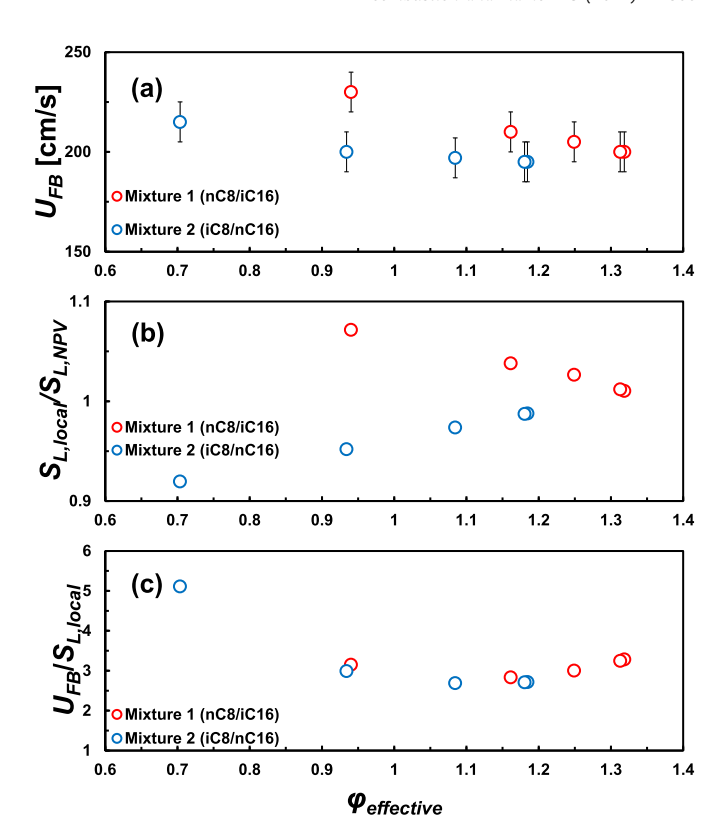


**Fig. 13.** Comparison of flashback behaviors for two mixtures with  $\varphi_{effective}$  at  $\varphi_g = 1.4$  in the partially vaporized condition (450 K); (a) the measured  $U_{FB}$  values, (b) the ratio of laminar flame speed  $(S_{L,local})$  considering preferential vaporization to the one  $(S_{L,NPV})$  without considering preferential vaporization, (c) the measured  $U_{FB}$  values normalized by local laminar flame speed  $(S_{L,local})$ .

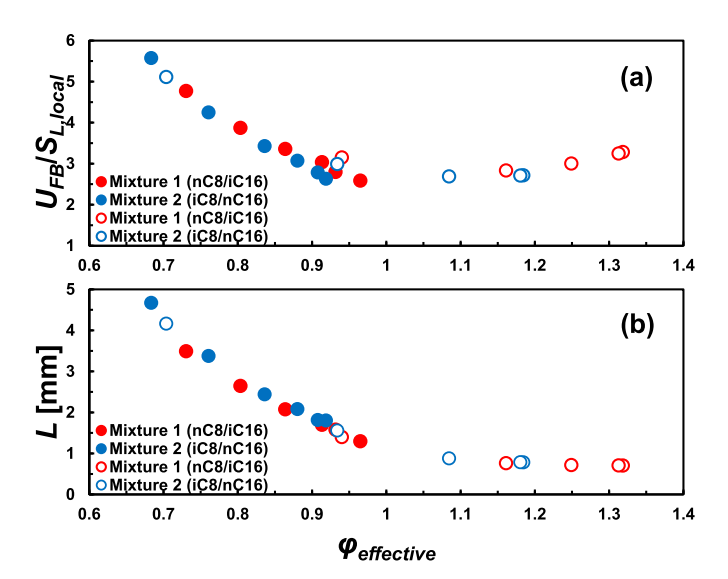


**Fig. 14.** (a) Consolidated results of  $U_{FB}$  normalized by  $S_{L,local}$  for both  $\varphi_g$  conditions, and (b) calculated Markstein length (L) as a function of  $\varphi_{effetive}$  in the partially vaporized condition (450 K). Closed symbols are for  $\varphi_g=1.0$  and open symbols are for  $\varphi_g=1.4$ .

cal flow velocity perturbations, compared to fuel-rich conditions. Since the premixed Bunsen flame is negatively stretched in general, the higher value of L in lean  $\varphi_{effetive}$  conditions would make the overall burning rate faster, thus resulting in the increase of  $U_{FB}/S_{L,local}$ . On the other hand, while the Markstein length monotonically decreases with  $\varphi_{effetive}$ , the  $U_{FB}/S_{L,local}$  value starts in-

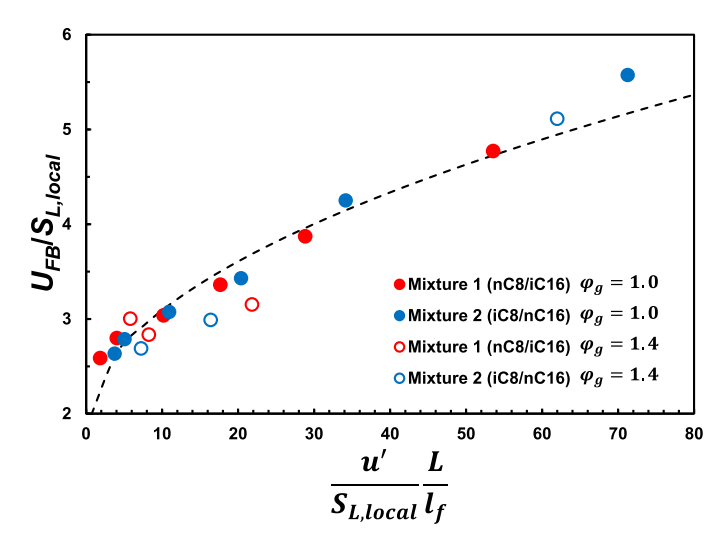


**Fig. 15.** Normalized  $U_{FB}$  by  $S_{L,local}$  as a function of  $u'L/S_{L,local}I_f$  in the partially vaporized condition (450 K). Closed symbols are for  $\varphi_{\rm g}=1.0$  and open symbols are for  $\varphi_{\rm g}=1.4$ .

creasing slightly again at  $\varphi_{effetive} > 1$ , which can be attributed to the onset of diffusive-thermal instability as shown in Fig. 11**d**.

Knowing that the overall burning rate is controlled by the interaction through the local flow stretch rate associated with Markstein length of the partially vaporized fuel/air mixture, Fig. 15 depicts the normalized  $U_{FB}$  by  $S_{L,local}$  as a function of  $u'L/S_{L,local}l_f$ . Here, the Markstein number  $(L/l_f)$  is multiplied to  $u'/S_{L,local}$  and the flame thickness  $(l_f)$  is calculated based on the thermal diffusivity and  $S_{L,local}$ . Following the Damköhler's hypothesis and assuming that  $U_{FB}/S_{L,lcoal}$  indicates the overall burning rate at flame flashback, a fitting equation can be derived as Eq. (3). Here, measurement points at the near-fully vaporized conditions are excluded from the fitting due to their unique behaviors caused by diffusive-thermal instability.

$$\frac{U_{FB}}{S_{L,local}} = 0.4 \left(\frac{u'}{S_{L,local}} \frac{L}{l_f}\right)^{\frac{1}{2}} + 1.85$$
 (3)

The derived fitting equation, Eq. (3), allows evaluating the relative contributions of laminar flame speed ( $S_{L,local}$ ), local flow velocity perturbation (u'), and preferential vaporization on the observed flame flashback behaviors by incorporating the normalized sensitivity coefficient. Since the local laminar flame speed is directly affected by the extent of fuel vaporization, the relative contribution of  $S_{L,local}$  can be regarded as the impact of fuel vapor deposition, defined as  $\frac{S_{L,local}}{U_{FB}} \frac{\partial U_{FB}}{\partial S_{L,local}}$ . The relative contribution of u' is defined as  $\frac{u'}{U_{FB}} \frac{\partial U_{FB}}{\partial u'}$ , which is introduced by the instantaneous fuel droplet vaporization. Finally, the relative contribution of preferential vaporization is determined as  $|\frac{\eta}{U_{FB}} \frac{\partial U_{FB}}{\partial \eta}|$  with  $\eta = \frac{S_{L,local} - S_{L,NPV}}{S_{L,NPV}}$  that compares the difference among the local laminar flame speeds with and without considering the preferential vaporization.

Fig. 16 compares the relative contributions of laminar flame speed, local flow perturbation, and preferential vaporization at the lowest extents of fuel vaporization of each measurement among two mixtures and two  $\varphi_g$  conditions. The results clearly suggest that the local laminar flame speed plays the most significant role on the flame flashback. The sensitivity to the local laminar flame speed includes both the impact of fuel vapor deposition (effective equivalence ratio) and that of preferential vaporization. However, the laminar flame speed varies only within 20% due to the predescribed mixtures composed of n- and iso-alkanes, whereas it varies considerably with the effective equivalence ratio controlled

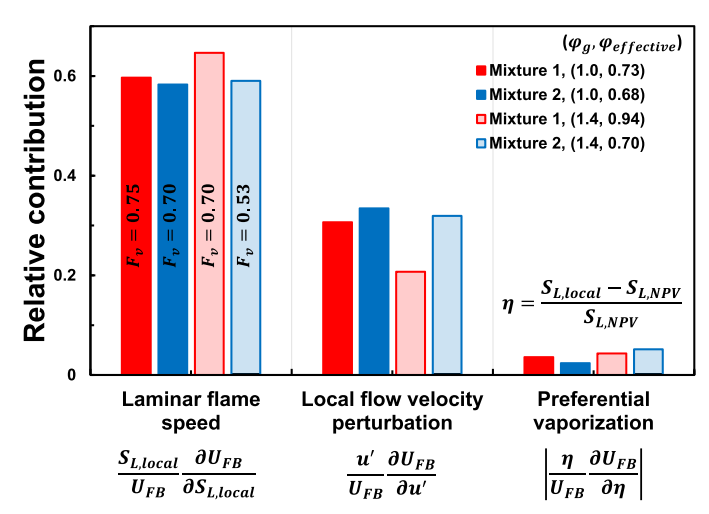


**Fig. 16.** Comparison of the relative contributions of laminar flame speed, local flow perturbation, and preferential vaporization based on sensitivity analysis.

by the extent of fuel vaporization. Thus, the sensitivity to the local laminar flame speed can be considered as representing mostly the impact of fuel vaporization. The contribution from local flow perturbation is found to be secondary in significance, diminishing in importance at the higher extent of fuel vaporization due to the reduced local fuel perturbation at near-fully vaporized conditions.

The contribution from preferential vaporization is found to be relatively weak in comparison, thus of second-order significance under the conditions tested. Its contribution increases with decreasing the extent of fuel vaporization, whereas it diminishes eventually full-vaporized conditions. Nevertheless, note that the impact of preferential vaporization is directly related to changes in local laminar flame speed as a result of the distillation characteristics. Only relatively moderate differences in laminar flame speeds are found for the two n-alkane/iso-alkane mixtures studied here (Figs. 12b and 13b) consistent with the noted, relatively weak dependence of flashback behaviors on preferential vaporization. However, the potential significance of preferential vaporization on flame flashback cannot be overlooked for cases such as considering the use of crude oil in gas turbine combustion [72–74]. In such a case, there is a much wider range of boiling temperatures combined with substantial differences in chemical functional group distribution over the distillation curve [75]. The present study evaluates the role of preferential vaporization on flame flashback behavior primarily governed by laminar flame speed that exhibits only moderate dependency on fuel chemical property (chemical kinetic potential). In the case of petroleum-derived jet fuels, the existence of aromatic components exclusively in the lighter fraction [19] would manifest considerable change of laminar flame speed over the distillation curve, thus the impact of preferential vaporization could be further magnified. For other combustion behaviors primarily controlled by flame extinction and/or ignition characteristics, the relative contribution of preferential vaporization could be further magnified due to the pronounced influence from fuel chemical properties. Considering the change of chemical properties in both petroleum-derived and alternative jet fuels with fuel boiling temperature in the distillation curve [19], it might be necessary to incorporate the preferential vaporization in high-fidelity surrogate formulation.

## 5. Conclusions

The impact of preferential vaporization on flame flashback behaviors was systematically investigated experimentally with a re-

cently developed spray burner that can vary the fraction of fuel vaporized from a well-defined droplet spray. Spray characteristics at the nozzle exit of the spray burner were determined by using the PDPA technique. The results show that the spray burner is capable of controlling the extent of fuel vaporization by changing the flow residence time from atomization to the burner surface and the temperature of incoming air. Flame flashback behaviors were determined at two conditions, fully- and partially vaporized conditions, by setting the burner temperature at 700 K and 450 K, respectively. The behaviors of four n-alkane fuels (n-heptane, n-octane, n-dodecane, and n-hexadecane) were compared against one another at fully vaporized conditions and results reveal a distinct flashback mechanism between propagation-driven and ignition-driven flashback mechanisms that depends on equivalence ratio.

To manifest the preferential vaporization impacts on flame flashback behaviors, two binary component fuel mixtures (noctane/iso-cetane and iso-octane/n-hexadecane mixtures) were formulated to share the same chemical functional group distributions for (CH<sub>2</sub>)<sub>n</sub> and CH<sub>3</sub>. At fully vaporized condition, the two binary component mixtures were found to exhibit almost identical flame flashback characteristics in both propagation- and ignition-driven flashback regimes, confirming the methodology applied to formulate the fuel mixtures.

The impact of preferential vaporization on flame flashback was then investigated using the two binary component mixtures at partially vaporized conditions (450 K of burner temperature). Experiments were performed at two global equivalence ratios and different extents of fuel vaporization were characterized by volume mean droplet diameter of fuel spray and its signal frequency measured with PDPA. The measurements enabled the estimation of the effective equivalence ratio resulting from the local fuel vapor deposition.

The measured mean jet velocities at flashback for the two binary component mixtures were found to differ due to the difference in local laminar flame speeds caused by the preferential vaporization characteristics. Considering observed wrinkled flame structure at flashback and that the experimental conditions fall within the wrinkled flamelet regime of the Borghi diagram, the influence of local flow velocity perturbation due to instantaneous droplet vaporization was evaluated from PDPA velocity fluctuation data. A pronounced increase in flashback velocity at leaner effective equivalence ratios was explained through differences in Markstein length and interpreting PLIF images.

Finally, the relative significance of local laminar flame speed, velocity perturbation, and preferential vaporization were determined through feature sensitivity analysis with a universal correlation that considers local laminar flame speed, local velocity fluctuation, and Markstein number. The results suggest that the local laminar flame speed and local velocity perturbation are of first-order significance in determining the flashback behaviors, while the impact of preferential vaporization is of second-order significance for the binary component fuel mixtures, n-octane/iso-cetane and iso-octane/n-hexadecane mixtures.

# **Declaration of Competing Interest**

The authors declare that they have no known competing financial interests or personal relationships that could have appeared to influence the work reported in this paper.

## Acknowledgments

This work is based upon work supported by the National Science Foundation under Grant No. 2028376. Any opinions, findings, and conclusions or recommendations expressed in this ma-

terial are those of the author(s) and do not necessarily reflect the views of the National Science Foundation. The development of the spray burner utilized under this study was partially supported by Siemens Energy Inc.

#### References

- T. Lieuwen, V. McDonell, E. Petersen, D. Santavicca, Fuel flexibility influences on premixed combustor blowout, flashback, autoignition, and stability, J. Eng. Gas Turb. Power. 130 (2008).
- [2] F.L. Dryer, Chemical kinetic and combustion characteristics of transportation fuels, Proc. Combust. Inst. 35 (2015) 117–144.
- [3] M. Stöhr, I. Boxx, C. Carter, W. Meier, Dynamics of lean blowout of a swirl-stabilized flame in a gas turbine model combustor, Proc. Combust. Inst. 33 (2011) 2953–2960.
- [4] A. Ateshkadi, V.G. McDonell, G.S. Samuelsen, Lean blowout model for a sprayfired swirl-stabilized combustor, Proc. Combust. Inst. 28 (2000) 1281–1288.
- [5] S.J. Shanbhogue, S. Husain, T. Lieuwen, Lean blowoff of bluff body stabilized flames: scaling and dynamics, Prog. Energy Combust. Sci. 35 (2009) 98–120.
- [6] T.C. Lieuwen, Unsteady Combustor Physics, Cambridge University Press, 2012.
- [7] W.-W. Kim, J.J. Lienau, P.R. Van Slooten, M.B. Colket, R.E. Malecki, S. Syed, To-wards Modeling Lean Blow Out in Gas Turbine Flameholder Applications, J. Eng. Gas Turb. Power. 128 (2004) 40–48.
- [8] M.B. Colket, J. Heyne, M. Rumizen, M. Gupta, A. Jardines, J.T. Edwards, W.M. Roquemore, G. Andac, R. Boehm, J. Zelina, J. Lovett, J. Condevaux, S. Bornstein, N. Rizk, D. Turner, C. Graves, M.S. Anand, R. Williams, Fang Xu, J.M. Tishkoff, C. Li, J.P. Moder, R. Anthenien, D. Friend, P. Chu, R. Kamin, Z. Haq, P. Serino, M. Domen, C.-B.M. Kweon, V. Sankaran, J. Cohen, W. Chishty, P. Canteenwalla, A. Corber, An overview of the national jet fuels combustion program, 54th AlAA Aerospace Sciences Meeting, American Institute of Aeronautics and Astronautics 2016.
- [9] L. Esclapez, P.C. Ma, E. Mayhew, R. Xu, S. Stouffer, T. Lee, H. Wang, M. Ihme, Fuel effects on lean blow-out in a realistic gas turbine combustor, Combust. Flame 181 (2017) 82–99.
- [10] A.H. Lefebvre, Fuel effects on gas turbine combustion Liner temperature, pattern factor and pollutant emissions, 20th Joint Propulsion Conference, American Institute of Aeronautics and Astronautics 1984.
- [11] A.H. Lefebvre, Fuel effects on gas turbine combustion—ignition, stability, and combustion efficiency, J. Eng. Gas Turb. Power. 107 (1985) 24–37.
- [12] ASTM D7566-21Specification for Aviation Turbine Fuel Containing Synthesized Hydrocarbons, ASTM International, West Conshohocken, PA, 2021.
- [13] S.H. Won, P.S. Veloo, S. Dooley, J. Santner, F.M. Haas, Y. Ju, F.L. Dryer, Predicting the global combustion behaviors of petroleum-derived and alternative jet fuels by simple fuel property measurements, Fuel 168 (2016) 34–46.
- [14] S.H. Won, N. Rock, S.J. Lim, S. Nates, D. Carpenter, B. Emerson, T. Lieuwen, T. Edwards, F.L. Dryer, Preferential vaporization impacts on lean blow-out of liquid fueled combustors, Combust. Flame 205 (2019) 295–304.
- [15] N. Rock, I. Chterev, B. Emerson, S.H. Won, J. Seitzman, T. Lieuwen, Liquid fuel property effects on lean blowout in an aircraft relevant combustor, J. Eng. Gas Turb. Power. 141 (2019) 071005–071005-071013.
- [16] S. Stouffer, T. Hendershott, J.R. Monfort, J. Diemer, E. Corporan, P. Wrzesinski, A.W. Caswell, Lean blowout and ignition characteristics of conventional and surrogate fuels measured in a swirl stabilized combustor, 55th AIAA Aerospace Sciences Meeting, American Institute of Aeronautics and Astronautics2017.
- [17] N. Rock, B. Emerson, J. Seitzman, T. Lieuwen, Near-lean blowoff dynamics in a liquid fueled combustor, Combust. Flame 212 (2020) 53–66.
- [18] J.G. Colborn, J.S. Heyne, S.D. Stouffer, T.H. Hendershott, E. Corporan, Chemical and physical effects on lean blowout in a swirl-stabilized single-cup combustor, Proc. Combust. Inst. 38 (2021) 6309–6316.
- [19] S. Nates, D. Carpenter, F.L. Dryer, S.H. Won, Preferential Vaporization Potential of Jet fuels Evaluated by NMR Spectroscopy, AIAA Scitech 2021 Forum.
- [20] A. Stagni, L. Esclapez, P. Govindaraju, A. Cuoci, T. Faravelli, M. Ihme, The role of preferential evaporation on the ignition of multicomponent fuels in a homogeneous spray/air mixture, Proc. Combust. Inst. 36 (2017) 2483–2491.
- [21] T.I. Farouk, S.H. Won, F.L. Dryer, Sub-millimeter sized multi-component jet fuel surrogate droplet combustion: physicochemical preferential vaporization effects, Proc. Combust. Inst. 38 (2021) 3313–3323.
- [22] V. Shastry, Q. Cazeres, B. Rochette, E. Riber, B. Cuenot, Numerical study of multicomponent spray flame propagation, Proc. Combust. Inst. 38 (2021) 3201–3211.
- [23] J.S. Heyne, E. Peiffer, M.B. Colket, A. Jardines, C. Shaw, J.P. Moder, W.M. Roquemore, J.T. Edwards, C. Li, M. Rumizen, M. Gupta, Year 3 of the national jet fuels combustion program: practical and scientific impacts of alternative jet fuel research, 2018 AIAA Aerospace Sciences Meeting, American Institute of Aeronautics and Astronautics2018.
- [24] B. Lewis, G.v. Elbe, Stability and structure of burner flames, J. Chem. Phys. 11 (1943) 75–97.
- [25] G.v. Elbe, M. Mentser, Further studies of the structure and stability of burner flames, J. Chem. Phys 13 (1945) 89–100.
- [26] S.L. Plee, A.M. Mellor, Review of flashback reported in prevaporizing/premixing combustors. Combust. Flame 32 (1978) 193–203.
- [27] Y. Sommerer, D. Galley, T. Poinsot, S. Ducruix, F. Lacas, D. Veynante, Large eddy simulation and experimental study of flashback and blow-off in a lean partially premixed swirled burner, J. Turbul. 5 (2004).

- [28] S.K. Dhanuka, J.E. Temme, J.F. Driscoll, H.C. Mongia, Vortex-shedding and mixing layer effects on periodic flashback in a lean premixed prevaporized gas turbine combustor, Proc. Combust, Inst. 32 (2009) 2901–2908.
- [29] B. Shaffer, Z. Duan, V. McDonell, Study of fuel composition effects on flashback using a confined jet flame burner, I. Eng. Gas Turb, Power. (2012) 135.
- [30] J. Kariuki, E. Mastorakos, Experimental investigation of turbulent flames in uniform dispersions of ethanol droplets, Combust. Flame 179 (2017) 95–116.
- [31] P.M. de Oliveira, P.M. Allison, E. Mastorakos, Ignition of uniform droplet-laden weakly turbulent flows following a laser spark, Combust. Flame 199 (2019) 387-400
- [32] M. Mikami, S. Miyamoto, N. Kojima, Counterflow diffusion flame with polydisperse sprays, Proc. Combust. Inst. 29 (2002) 593–599.
- [33] J.T. Zung, Evaporation rate and lifetimes of clouds and sprays in air—The Cellular Model, J. Chem. Phys. 46 (1967) 2064–2070.
- [34] J.M. Tishkoff, A model for the effect of droplet interactions on vaporization, Int. J. Heat Mass Transf. 22 (1979) 1407–1415.
- [35] S.H. Won, F.M. Haas, S. Dooley, T. Edwards, F.L. Dryer, Reconstruction of chemical structure of real fuel by surrogate formulation based upon combustion property targets, Combust. Flame 183 (2017) 39–49.
- [36] S.H. Won, F.M. Haas, A. Tekawade, G. Kosiba, M.A. Oehlschlaeger, S. Dooley, F.L. Dryer, Combustion characteristics of C4 iso-alkane oligomers: experimental characterization of iso-dodecane as a jet fuel surrogate component, Combust. Flame 165 (2016) 137–143.
- [37] S.H. Won, S. Dooley, P.S. Veloo, H. Wang, M.A. Oehlschlaeger, F.L. Dryer, Y. Ju, The combustion properties of 2,6,10-trimethyl dodecane and a chemical functional group analysis, Combust. Flame 161 (2014) 826–834.
- [38] D. Carpenter, S. Nates, F.L. Dryer, S.H. Won, Evaluating ignition propensity of high cycloparaffinic content alternative jet fuel by a chemical functional group approach, Combust. Flame 223 (2021) 243–253.
- [39] K. Dussan, S.H. Won, A.D. Ure, F.L. Dryer, S. Dooley, Chemical functional group descriptor for ignition propensity of large hydrocarbon liquid fuels, Proc. Combust. Inst. 37 (2019) 5083–5093.
- [40] S. Dooley, S.H. Won, S. Jahangirian, Y. Ju, F.L. Dryer, H. Wang, M.A. Oehlschlaeger, The combustion kinetics of a synthetic paraffinic jet aviation fuel and a fundamentally formulated, experimentally validated surrogate fuel, Combust. Flame 159 (2012) 3014–3020.
- [41] S. Dooley, S.H. Won, J. Heyne, T.I. Farouk, Y. Ju, F.L. Dryer, K. Kumar, X. Hui, C.-J. Sung, H. Wang, M.A. Oehlschlaeger, V. Iyer, S. Iyer, T.A. Litzinger, R.J. Santoro, T. Malewicki, K. Brezinsky, The experimental evaluation of a methodology for surrogate fuel formulation to emulate gas phase combustion kinetic phenomena, Combust. Flame 159 (2012) 1444–1466.
- [42] S. Dooley, S.H. Won, M. Chaos, J. Heyne, Y. Ju, F.L. Dryer, K. Kumar, C.--J. Sung, H. Wang, M.A. Oehlschlaeger, R.J. Santoro, T.A. Litzinger, A jet fuel surrogate formulated by real fuel properties, Combust. Flame 157 (2010) 2333–2339.
- [43] D. Kim, J. Martz, A. Violi, A surrogate for emulating the physical and chemical properties of conventional jet fuel, Combust. Flame 161 (2014) 1489–1498.
- [44] S.T. Lee, J.S. T'len, A numerical analysis of flame flashback in a premixed laminar system, Combust. Flame 48 (1982) 273–285.
- [45] V. Kurdyumov, E. Fernández-Tarrazo, J.M. Truffaut, J. Quinard, A. Wangher, G. Searby, Experimental and numerical study of premixed flame flashback, Proc. Combust. Inst. 31 (2007) 1275–1282.
- [46] S.H. Won, B. Windom, B. Jiang, Y. Ju, The role of low temperature fuel chemistry on turbulent flame propagation, Combust. Flame 161 (2014) 475–483.
- [47] B. Windom, S.H. Won, C.B. Reuter, B. Jiang, Y. Ju, S. Hammack, T. Ombrello, C. Carter, Study of ignition chemistry on turbulent premixed flames of n-heptane/air by using a reactor assisted turbulent slot burner, Combust. Flame 169 (2016) 19–29.
- [48] J. Yanowitz, M.A. Ratcliff, R.L. McCormick, J.D. Taylor, M.J. Murphy, Compendium of Experimental Cetane Numbers, NREL (National Renewable Energy Laboratory (NREL), Golden, CO (United States)), 2017.
- [49] S.M. Sarathy, C.K. Westbrook, M. Mehl, W.J. Pitz, C. Togbe, P. Dagaut, H. Wang, M.A. Oehlschlaeger, U. Niemann, K. Seshadri, P.S. Veloo, C. Ji, F.N. Egolfopoulos, T. Lu, Comprehensive chemical kinetic modeling of the oxidation of 2-methy-lalkanes from C7 to C20, Combust. Flame 158 (2011) 2338–2357.
- [50] E. Ranzi, A wide-range kinetic modeling study of oxidation and combustion of transportation fuels and surrogate mixtures, Energ. Fuel 20 (2006) 1024–1032.
- [51] H.-P.S. Shen, J. Steinberg, J. Vanderover, M.A. Oehlschlaeger, A shock tube study of the ignition of n-heptane, n-decane, n-dodecane, and n-tetradecane at elevated pressures, Energ. Fuel 23 (2009) 2482–2489.

- [52] K. Zhang, C. Banyon, U. Burke, G. Kukkadapu, S.W. Wagnon, M. Mehl, H.J. Curran, C.K. Westbrook, W.J. Pitz, An experimental and kinetic modeling study of the oxidation of hexane isomers: developing consistent reaction rate rules for alkanes, Combust. Flame 206 (2019) 123–137.
- [53] C. Ji, S.M. Sarathy, P.S. Veloo, C.K. Westbrook, F.N. Egolfopoulos, Effects of fuel branching on the propagation of octane isomers flames, Combust. Flame 159 (2012) 1426–1436.
- [54] C.K. Westbrook, W.J. Pitz, H.C. Curran, J. Boercker, E. Kunrath, Chemical kinetic modeling study of shock tube ignition of heptane isomers, Int. J. Chem. Kinet. 33 (2001) 868–877.
- [55] B. Abramzon, W.A. Sirignano, Droplet vaporization model for spray combustion calculations, Int. J. Heat Mass Transf. 32 (1989) 1605–1618.
- [56] W.A. Sirignano, Fuel droplet vaporization and spray combustion theory, Prog. Energy Combust. Sci. 9 (1983) 291–322.
- [57] J.H. Burgoyne, L. Cohen, D.M. Newitt, The effect of drop size on flame propagation in liquid aerosols, Proc. R. Soc. London, Ser. A 225 (1954) 375–392.
- [58] Y. Nunome, S. Kato, K. Maruta, H. Kobayashi, T. Niioka, Flame propagation of n-decane spray in microgravity, Proc. Combust. Inst. 29 (2002) 2621–2626.
- [59] S. Hayashi, T. Ohtani, K. Jinuma, S. Kumagai, Limiting factor of flame propagation in low-volatility fuel clouds, Symp. (Int.) Combust. 18 (1981) 361–367.
- [60] D. Bradley, M. Lawes, S. Liao, A. Saat, Laminar mass burning and entrainment velocities and flame instabilities of i-octane, ethanol and hydrous ethanol/air aerosols, Combust. Flame 161 (2014) 1620–1632.
- [61] R. Thimothée, C. Chauveau, F. Halter, I. Gökalp, Experimental investigation of the mechanisms of cellular instabilities developing on spherical two-phase flames, Combust. Sci. Technol. 188 (2016) 2026–2043.
- [62] R. Thimothée, C. Chauveau, F. Halter, I. Gökalp, Experimental investigation of the passage of fuel droplets through a spherical two-phase flame, Proc. Combust. Inst. 36 (2017) 2549–2557.
- [63] S. Kadowaki, T. Hasegawa, Numerical simulation of dynamics of premixed flames: flame instability and vortex-flame interaction, Prog. Energy Combust. Sci. 31 (2005) 193–241.
- [64] S. Dooley, S.H. Won, F.M. Haas, J. Santner, Y. Ju, F.L. Dryer, T.I. Farouk, Development of reduced kinetic models for petroleum-derived and alternative jet fuels, 50th AIAA/ASME/SAE/ASEE Joint Propulsion Conference, 2014.
- [65] N. Peters, The turbulent burning velocity for large-scale and small-scale turbulence, J. Fluid Mech. 384 (1999) 107–132.
- [66] R. Borghi, On the structure and morphology of turbulent premixed flames, in: C. Casci, C. Bruno (Eds.), Recent Advances in the Aerospace Sciences: In Honor of Luigi Crocco on His Seventy-fifth Birthday, Springer US, Boston, MA (1985), pp. 117–138.
- [67] M.Z. Haq, C.G.W. Sheppard, R. Woolley, D.A. Greenhalgh, R.D. Lockett, Wrinkling and curvature of laminar and turbulent premixed flames, Combust. Flame 131 (2002) 1–15.
- [68] J.F. Driscoll, Turbulent premixed combustion: flamelet structure and its effect on turbulent burning velocities, Prog. Energy Combust. Sci 34 (2008) 91–134.
- [69] C.J. Sun, C.J. Sung, L. He, C.K. Law, Dynamics of weakly stretched flames: quantitative description and extraction of global flame parameters, Combust. Flame 118 (1999) 108–128.
- [70] J.K. Bechtold, M. Matalon, The dependence of the Markstein length on stoichiometry, Combust. Flame 127 (2001) 1906–1913.
- [71] R. Addabbo, J.K. Bechtold, M. Matalon, Wrinkling of spherically expanding flames, Proc. Combust. Inst. 29 (2002) 1527–1535.
- [72] J. Goldmeer, R. Symonds, P. Glaser, B. Mohammad, Z. Nagel, P. Perez-Diaz, Evaluation of arabian super light crude oil for use in a F-Class DLN combustion system, ASME Turbo Expo 2014: Turbine Technical Conference and Exposition, 2014.
- [73] K. Tada, K. Inoue, T. Kawakami, K. Saitoh, S. Tanimura, Expanding fuel flexibility in MHPS' dry low NOx combustor, ASME Turbo Expo 2018: Turbomachinery Technical Conference and Exposition, 2018.
- [74] S.C. Gülen, Gas Turbines for Electric Power Generation, Cambridge University Press, 2019.
- [75] S.H. Won, S.J. Lim, S. Nates, A.K. Alwahaibi, F.L. Dryer, F. Farid, M. Hase, Combustion characteristics of crude oils for gas turbine applications by DCN measurements and NMR spectroscopy, Proc. Combust. Inst. 38 (2021) 5463–5473.